Operating-point-dependent measurement uncertainty analysis of performance indicators for a high-temperature heat pump

Felix Muntel[a, b,*], Simon Höckenkamp[b], Michael Rath[a, b]

[a.]Bochum University of Applied Sciences, Bochum, North Rhine-Westphalia, Germany,
[b.] Fraunhofer Research Institution for Energy Infrastructures and Geotechnologies IEG, Bochum, North Rhine-Westphalia, Germany

**Corresponding Author felix.muntel@stud.hs-bochum.de*

Keywords: High-temperature heat pump, measurement uncertainty, coefficient of performance, Gaussian error propagation, natural refrigerant, R718

Abstract

Reliable performance assessment of high-temperature heat pumps (HTHPs) requires not only accurate measurements but also a systematic understanding of measurement uncertainties and their dependence on operating conditions. This paper presents an operating-point-dependent measurement uncertainty analysis of key performance indicators for a high-temperature heat pump developed within the SteamScrew research project, which investigates water as a natural refrigerant combined with a water-injected single-stage screw compressor.

The study focuses on the influence of sensor selection and sensor sizing on the uncertainty of experimentally determined performance indicators, namely the coefficient of performance (COP), the Carnot COP, and the Carnot efficiency. Measurement uncertainties are quantified using analytical Gaussian error propagation based on the full measurement chain, including temperature sensors (PT100), Coriolis mass flow meters, and electrical power measurement via current transformers. The analysis is applied to multiple representative operating points covering a wide range of sink temperature differences and mass flow rates.

Results show that the total relative measurement uncertainty of the COP ranges between ±1.14 % and ±1.6 %, depending on the operating point. A sensitivity analysis reveals that temperature measurements dominate the overall uncertainty at small temperature differences, highlighting the critical role of sensor class, placement, and resolution. In contrast, electrical power measurement uncertainties become significant when current transformers operate far from their nominal range, emphasizing the importance of proper sensor dimensioning. The findings demonstrate that sensor oversizing can degrade measurement accuracy under partial-load conditions.

The paper highlights that measurement uncertainty is not a fixed property of the test rig but strongly depends on the interaction between operating conditions and sensor design. The results provide practical guidance for the selection and dimensioning of sensors in HTHP facilities. Beyond the presented bachelor thesis framework, the findings are directly relevant for the ongoing development of the SteamScrew test rig and offer transferable insights for future experimental research on high-temperature heat pump systems.

1. Introduction

The decarbonization of industrial heat supply is one of the central challenges of the energy transition. Industrial processes account for 20–25 % of total final energy consumption in Europe, with a large share attributable to process heat at temperatures above 100 °C [1]. HTHPs represent a promising technology to address this demand, as they can provide thermal energy at temperatures well above 100 °C with significantly higher energy efficiency compared to conventional combustion-based systems or direct electric solutions [2]. Sectors such as the paper, food, and chemical industries require process heat at temperatures of up to 200 °C, a range that is now within reach for state-of-the-art HTHPs [2].

Despite this potential, the reliable experimental characterization of HTHP performance remains challenging. One key performance indicator of any heat pump is the COP, defined as the ratio of useful heat output to the

electrical input power of the compressor. In experimental settings, the COP and related performance metrics are derived from a chain of measured quantities, including temperatures, mass flow rates, and electrical power. Each subject includes individual measurement uncertainties. These uncertainties propagate through the calculation and introduce an overall uncertainty band around the reported performance figures. Without a quantification of this uncertainty, the comparability of experimental results across different test facilities and the reliability of conclusions drawn from measured data remain limited [3].

The present work is conducted within the framework of the joint research project SteamScrew, which aims to develop a HTHP for industrial applications using water as the natural refrigerant. Water offers several advantages in this context: Water is non-flammable, environmentally benign, widely available, and possesses favorable thermodynamic properties at the required pressure and temperature levels [2]. The SteamScrew concept employs a single-stage oil-free screw compressor with liquid water injection to manage compressor outlet temperatures. The project targets source temperatures in the range of 80–130 °C which is representative of industrial waste heat and geothermal resources and aims to deliver process heat at sink temperatures between 140 °C and 200 °C [4]. The test rig is operated at the Fraunhofer IEG in Bochum, Germany, with a maximum compressor input power of 220 kW.

Within this project, the present study develops an analytical tool for the operating-point-dependent quantification of measurement uncertainties for three performance indicators which are the COP, the Carnot COP, and the Carnot efficiency. The analysis is based on Gaussian error propagation applied to the full measurement chain, encompassing Coriolis mass flow meters, PT100 resistance temperature sensors, current transformers, and associated signal conditioning hardware. Six representative operating points, derived from simulation results reported by Höckenkamp et al. [5], serve as the basis for the numerical evaluation. A subsequent sensitivity analysis systematically identifies the dominant uncertainty contributors across the sensor chain.

The paper is structured as follows: Section 2 describes the SteamScrew test rig, its instrumentation, and the measurement chain. Section 3 presents the performance metrics and the mathematical framework for uncertainty propagation. Section 4 details the uncertainty analysis and the derivation of operating-point-dependent uncertainty functions. Section 5 reports and discusses the results, including a comparison with published data from comparable systems. Section 6 summarizes the findings and formulates recommendations for future measurement campaigns.

2. System description

This section describes the SteamScrew test rig that forms the experimental basis of the present study. The description covers the thermodynamic layout of the heat pump circuit, the key characteristics of the screw compressor, and the full measurement chain installed at the Fraunhofer IEG.

2.1 The SteamScrew heat pump circuit

The SteamScrew test rig implements a vapor-compression heat pump cycle using water as the working fluid. The heat pump is designed for source-side inlet temperatures of 80–130 °C, supplied via a source circuit connected to the evaporator through a plate-and-shell heat exchanger. On the sink side, the thermal energy is transferred to the process fluid across two condensers arranged in series. Each condenser is instrumented with inlet and outlet temperature sensors as well as a Coriolis mass flow meter, allowing the total heat output to be determined from both condensers independently. The sink circuit is maintained at a system pressure of 20 bar. After leaving the condensers, the liquid refrigerant enters a separator tank that ensures a continuous liquid supply to the expansion valve. A bypass line downstream the separator tank routes a fraction of the refrigerant back to the compressor. Along this path, the refrigerant from the separator tank is injected into the compressor for colling purposes during compression.

2.2 The twin-screw compressor

The core component of the SteamScrew system is a twin-screw compressor developed by Aerzener Maschinenfabrik GmbH specifically for single-stage compression of water vapor with simultaneous liquid injection. The machine consists of two intermeshing helical rotors whose counterrotation generates working chambers along the rotor axis. Saturated vapor entering at the low-pressure side is transported towards the high-pressure outlet and compressed [6]. The compressor is driven by an electric motor via a frequency converter (FC), enabling variable-speed operation. Three current transformers, one per phase of the three-phase supply cable between power supply and the FC, measure the individual phase currents to determine the total electrical input power. This arrangement includes FC losses within the measured power, consistent with the system boundary chosen for the COP definition.

2.3 Instrumentation and measurement chain

The measurement chain comprises three physical quantities including temperatures, mass flow rates, and electrical power. Table 1 summarizes the sensors and signal conditioning hardware used for each quantity together with their manufacturer-specified uncertainties.

Table 1. Instrumentation of the SteamScrew test rig.

Measured quantity	Instrument	Type	Range	Uncertainty
Sink temperatures	PT100 temp. sensor	Class AA (DIN EN IEC 60751)	−50 to +250 °C (cal. 160 °C)	±(0.1 + 0.0017|t|) K
Source inlet temp.	PT100 temp. sensor	Class AA (DIN EN IEC 60751)	−50 to +250 °C (cal. 100 °C)	±(0.1 + 0.0017|t|) K
Mass flow rates	Coriolis meter (CMD)	E+H Proline Promass F 100	0–15 000 kg/h	Operating-point-dependent (Sec. 4)
Specific heat capacity cp	CoolProp library [8]	IAPWS-IF97 [9]	100–200 °C, 20 bar	±0.5 %
Electrical power	Current transformer	AcuCT-S220-1200:5 (Accuenergy)	0–220 kW	Operating-point-dependent (IEC 61869-2)
Electrical power (meter)	Power meter	Acuvim-CL-D-5A-P1V4 (Accuenergy)	0–220 kW	±0.5 %

Temperatures are measured by Class AA PT100 platinum resistance thermometers calibrated at 160 °C (sink side) and 100 °C (source side). Each PT100 signal is fed into a Siemens SIMATIC ET 200SP AI 8xRTD/TC temperature measurement card (base uncertainty ±0.05 %, temperature coefficient ±0.0009 %/K). The mass flow rates in both sink circuits are measured by calibrated Coriolis meters. Above 20 % of the rated flow the uncertainty is below ±0.03 % from the calibration certificate, rising steeply below this threshold. The CMD output is digitized by a Siemens SIMATIC ET 200SP F-AI 4x1 signal card (base uncertainty ±0.1 %, temperature coefficient ±0.023 %/K). The rated primary current of the current transformers is 1200 A, yet the maximum motor current at full compressor load is approximately 409 A which is 34 % of the rated value. This is resulting in an elevated relative uncertainty at partial loads that is analyzed in detail in Section 5.

3. Performance metrics and methodology

This section defines the three performance indicators investigated in this study, derives the measurement functions that connect them to the directly observable sensor quantities, and introduces the Gaussian error propagation framework used to quantify their combined measurement uncertainties.

3.1 Coefficient of performance

The COP of a heat pump is the ratio of the useful thermal power delivered at the condenser to the electrical power consumed by the compressor drive [7].

$$COP = \frac{\dot{Q}_{out}}{P_{el}} \tag{1}$$

$\dot{Q}out$ is the total thermal power transferred to the sink circuit and Pel is the electrical input power of the compressor motor including frequency converter losses. Because the SteamScrew test rig features two condensers operating in parallel on the sink side, the total heat output is the sum of the individual condenser contributions. The thermal power of each condenser is calculated from the calorimetric equation.

$$\dot{Q}_{out} = \dot{m}_1 \cdot c_{p,1} \cdot (T_{out,S1} - T_{in,S1}) + \dot{m}_2 \cdot c_{p,2} \cdot (T_{out,S2} - T_{in,S2}) \tag{2}$$

Where m_i is the mass flow rate at condenser i, $c_{p,i}$ is the specific heat capacity of the sink fluid at condenser i evaluated using CoolProp [8] at the mean temperature and a constant pressure of 20 bar, and $T_{out,Si}$ and $T_{in,Si}$ are the sink outlet and inlet temperatures at condenser i, respectively. Combining Eqs. (1) and (2) yields the full COP measurement function.

$$COP = \frac{\dot{m}_1 \cdot c_{p,1} \cdot (T_{out,S1} - T_{in,S1}) + \dot{m}_2 \cdot c_{p,2} \cdot (T_{out,S2} - T_{in,S2})}{P_{el}} \text{ [-]} \tag{3}$$

This expression contains nine independent input quantities, each subject to its own measurement uncertainty including the two mass flow rates, two specific heat capacities, four temperatures, and the electrical power.

3.2 Carnot COP

The Carnot COP is the upper thermodynamic limit of the COP for a heat pump operating between two fixed temperature reservoirs [7]. It depends on the sink outlet temperature and the source inlet temperature, both in Kelvin.

$$COP_{Carnot} = \frac{T_{out,S}}{T_{out,S} - T_{in,Q}} \text{ [-]} \tag{4}$$

$T_{out,S}$ is the mean sink outlet temperature and $T_{in,Q}$ is the source circuit inlet temperature. Eq. (4) involves two measured quantities, which results in lower overall measurement uncertainty as shown in Section 5.

3.3 Carnot efficiency

The Carnot efficiency η_{Carnot} is the ratio of the measured COP to the Carnot COP.

$$\eta_{Carnot} = \frac{COP}{COP_{Carnot}} \text{ [-]} \tag{5}$$

This dimensionless indicator quantifies how closely the real cycle approaches the ideal reversible limit. Typical values for compression heat pumps lie in the range 0.4–0.6 [2].

3.4 Gaussian error propagation

All three performance indicators are computed from multiple directly measured quantities, each carrying an individual measurement uncertainty. For a derived quantity $y = f(x_1, x_2, \dots, x_n)$ that is a differentiable function of n statistically independent input quantities x_i, the combined standard uncertainty $u(y)$ is given [9].

$$u(y) = \sqrt{(\sum_i \frac{\partial f}{\partial x_i} u(x_i))^2} \tag{6}$$

The partial derivative $\frac{\partial f}{\partial x_i}$ is the sensitivity coefficient of y with respect to input x_i, and $u(x_i)$ is the standard uncertainty of x_i. For quantities, whose measurement chain consists of two serially connected components, for example, a PT100 sensor followed by a temperature measurement card, the combined uncertainty of that sub-chain is itself computed by Gaussian propagation before being substituted into Eq. (6). All partial derivatives are treated as absolute values to prevent artificial cancellation of uncertainty contributions.

For Carnot efficiency, since $u(COP)$ and $u(COP_{Carnot})$ are the fully propagated standard uncertainties of the two intermediate quantities, Eq. (6) applied to Eq. (5) is shown in Eq. (7).

$$u(\eta_{Carnot}) = \sqrt{(\frac{\partial \eta_{Carnot}}{\partial COP} u(COP))^2 + (\frac{\partial \eta_{Carnot}}{\partial COP_{Carnot}} u(COP_{Carnot}))^2} \text{ [-]} \tag{7}$$

The approach accounts for random measurement uncertainties only. Systematic biases such as long-term sensor drift or electromagnetic interference are not included in the present analysis. All uncertainty functions have been implemented in an Excel-based calculation tool that evaluates the full propagation chain for any given operating point.

4. Measurement uncertainty analysis

This section derives the operating-point-dependent uncertainty functions for each element of the measurement chain and assembles them into the combined standard uncertainties of the three performance indicators. The analysis follows the two-level propagation strategy introduced in Section 3. Therefore, individual sensor uncertainties are first combined within each measurement sub-chain (sensor plus signal conditioning card), and the resulting combined sub-chain uncertainties are then propagated through the performance indicator functions.

4.1 Operating conditions and boundary assumptions

The boundary conditions for the uncertainty analysis are derived from the simulated operating range reported by Höckenkamp et al. [5]. The boundaries are source inlet temperatures of 80–130 °C, sink outlet temperatures of 140–210 °C, total sink-side mass flow rates of 1.7–7.4 kg/s, and compressor input powers of 45–200 kW. These ranges define the envelope within which all operating-point-dependent sensor uncertainties are evaluated.

The following simplifying assumptions are adopted throughout. The pressure of the sink circuit is treated as a known constant (20 bar), and its uncertainty is not propagated into the specific heat capacity. The specific heat

capacity of the sink fluid is computed by CoolProp [8] from the local temperature at each condenser. Its uncertainty is fixed at ±0.5 % in accordance with Wagner and Pruß [9]. Auxiliary electrical consumers (pumps, actuators) are excluded from the power balance. Their combined power is small relative to the compressor motor, and their omission introduces a systematic COP overestimation that is noted as a limitation rather than propagated as a random uncertainty.

4.2 Temperature measurement sub-chain

Each temperature in the measurement chain is measured by a PT100 Class AA sensor whose uncertainty is defined according to DIN EN IEC 60751 [10].

$$u(PT100) = \pm(0.1 + 0.0017 \cdot |\Delta T|) \text{ [K]} \tag{8}$$

In this case ΔT is the deviation of the measured temperature from the calibration reference temperature of the respective sensor (160 °C for sink-side sensors, 100 °C for the source-side sensor). The minimum uncertainty of ±0.1 °C applies at the calibration point and increases linearly with deviation from it. The analogue PT100 signal is digitized by the Siemens temperature card. The combined uncertainty looks like this.

$$u(T - card) = \pm(0.05 + 0.0009 \cdot |Topt\ -\ 25|) \text{ [%]} \tag{9}$$

In this scenario T_{opt} is the optimal temperature of the temperature card. At the assumed operating temperature of 40 °C, this is evaluated to 0.0635 %. Next is the combined standard uncertainty of each temperature measurement sub-chain.

$$u(T) = \sqrt{\left(u(PT100)\right)^2 + \left(u(T - card)\right)^2} \text{ [K]} \tag{10}$$

Since $u(PT100)$ is expressed in K and $u(T - card)$ as a percentage of the measured value, the PT100 uncertainty is converted to a percentage of the measured temperature before quadratic combination. The key sensitivity driver in this sub-chain is $u(PT100)$, which grows rapidly when the operating temperature deviates from the calibration point, and becomes especially significant when temperature differences are considered (e.g. for calculating heating powers). Especially for decreasing temperature differences. This finding dominates the sensitivity analysis in Section 5.

4.3 Mass flow measurement sub-chain

The Coriolis meters are calibrated instruments whose uncertainty characteristics are described by a manufacturer calibration certificate. In the calibrated range (flow fraction φ ≥ 20 % of maximum rated flow), linear interpolation between five calibration points yields uncertainties between −0.03 % and +0.01 %. Below the calibration threshold (φ < 20 %), the uncertainty increases steeply and is approximated by a power-law function fitted to the manufacturer's characteristic diagram.

$$u(CMD, \varphi < 20\%) = \pm\frac{19.2}{\varphi^{2.39}} + 0.1 \text{ [%]} \tag{11}$$

In this situation φ is the flow fraction in percent. The fit function fits the manufacturers data and the maximum deviation between the fitted function and the tabulated values is less than 0.1 percentage points across the range 3 – 20 %. The expected operating range of the SteamScrew test rig corresponds to flow fractions of 14 – 49 % for the two CMDs, placing all normal operating points within the calibrated range and resulting in CMD uncertainties below ±0.3 %.

The CMD analogue output signal (4–20 mA) is digitized by the Siemens F-AI signal card with combined uncertainty that is shown in Eqs. (12).

$$u(CMD - card) = \pm(0.1 + 0.023 \cdot |T_{opt} - 25|) \text{ [%]} \tag{12}$$

The cabinets are climate-controlled to keep the temperature of the measurement cards close to the ideal temperatures which is 25 °C. At 40 °C cabinet temperature, which corresponds to a worst-case scenario, this yields ±0.445 %. The combined standard uncertainty of the mass flow sub-chain can be seen in Eqs. (13).

$$u(\dot{m}) = \sqrt{\left(u(CMD)\right)^2 + (u(CMD - card))^2} \text{ [kg/s]} \tag{13}$$

At normal operating conditions, the CMD-card uncertainty (±0.445 %) dominates over the calibrated CMD uncertainty (< ±0.03 %), making the signal conditioning card the primary contributor to mass flow measurement uncertainty.

4.4 Electrical power measurement sub-chain

The electrical input power is determined from three current transformers and a power meter. The three current transformers operate independently and contribute uncorrelated uncertainties, and their combined variance contribution is therefore three times the variance of a single transformer. The transformer uncertainty is defined according to IEC 61869-2 [11] as a function of the load fraction relative to the rated primary current (1200 A). Linear interpolation between the four normalized load points given by the manufacturer yields is shown in Table 2.

Table 2. Current transformer uncertainty per IEC 61869-2 [11]

Load fraction (% of rated current)	Transformer uncertainty (%)
5	0,75
20	0,35
100	0,2
120	0,2

At the maximum compressor load (409 A, corresponding to 34 % of the rated current of 1200 A), the transformer uncertainty evaluates to ±0.32 % by linear interpolation. It follows the combined standard uncertainty of the electrical power measurement sub-chain, including three transformers and the power meter.

$$u(Pel) = \sqrt{3\big(u(CT)\big)^2 + (u(meter))^2} \text{ [W]} \tag{14}$$

$u(CT)$ is the transformer uncertainty at the prevailing load fraction and $u(meter) = \pm 0.5\%$ is the fixed power meter uncertainty. At the design-point load fraction of 34 %, Eq. (14) yields $u(Pel) \approx \pm 0.63\%$. This is the dominant contribution to the COP uncertainty from the denominator of Eq. (3) and is larger than it would be with a transformer sized to the actual motor current.

4.5 Combined uncertainty of the COP

The combined standard uncertainty of the COP is obtained by applying Eq. (6) to Eq. (3). The nine partial derivatives of the COP with respect to the input quantities are evaluated analytically.

$$\frac{\partial COP}{\partial \dot{m}_\iota} = \frac{c_{p,i} \cdot (T_{out,S,i} - T_{in,S,i})}{P_{el}} \tag{15}$$

$$\frac{\partial COP}{\partial c_{p,i}} = \frac{\dot{m}_\iota \cdot (T_{out,S,i} - T_{in,S,i})}{P_{el}} \tag{16}$$

$$\frac{\partial COP}{\partial T_{out,S,i}} = \frac{\dot{m}_\iota \cdot c_{p,i}}{P_{el}} \tag{17}$$

$$\frac{\partial COP}{\partial T_{in,S,i}} = -\frac{\dot{m}_\iota \cdot c_{p,i}}{P_{el}} \tag{18}$$

$$\frac{\partial COP}{\partial P_{el}} = -\frac{\dot{m}_\iota \cdot c_{p,i} \cdot (T_{out,S,i} - T_{in,S,i})}{{P_{el}}^2} \tag{19}$$

Substituting these sensitivity coefficients together with the sub-chain uncertainties from Eqs. (10), (13), and (14) into Eq. (6) yields the combined standard uncertainty $u(COP)$. The negative sign in Eqs. (18) and (19) is replaced by the absolute value in the propagation, ensuring that all contributions add in quadrature regardless of sign.

4.6 Combined uncertainty of the Carnot COP

The uncertainty of the Carnot COP follows from Eq. (6) applied to Eq. (4). With only two input quantities, the partial derivatives are the following.

$$\frac{\partial COP_{Carnot}}{\partial T_{out,S}} = -\frac{T_{in,Q}}{(T_{out,S} - T_{in,Q})^2} \tag{20}$$

$$\frac{\partial COP_{Carnot}}{\partial T_{in,Q}} = \frac{T_{out,S}}{(T_{out,S} - T_{in,Q})^2} \tag{21}$$

Next is the combined uncertainty.

$$u(COP_{Carnot}) = \sqrt{\left(\frac{\partial COP_{Carnot}}{\partial T_{out,S}} \cdot u\left(T_{out,S}\right)\right)^2 + \left(\frac{\partial COP_{Carnot}}{\partial T_{in,Q}} \cdot u\left(T_{in,Q}\right)\right)^2} \quad (22)$$

4.7 Combined uncertainty of the Carnot efficiency

The Carnot efficiency uncertainty is obtained directly from Eq. (7) using the propagated results of Sections 4.5 and 4.6. No further partial differentiation is required since $u(COP)$ and $u(COP_{Carnot})$ already represent fully propagated standard uncertainties. The dominant contribution to $u(\eta_{Carnot})$ comes from $u(COP)$, since the uncertainty of the Carnot COP is typically smaller. This is a consequence of the limited number of input quantities and the high accuracy of the PT100 sensors at moderate temperature differentials.

5. Results and discussion

The measurement uncertainty model developed in Section 4 was applied to six representative operating points of the SteamScrew test rig, spanning the full range of anticipated source temperatures (80–130 °C), sink temperatures (140–200 °C), mass flow rates (1.7–7.4 kg/s), and compressor input powers (45–200 kW). For each operating point, the Excel-based calculation tool evaluates all sensor uncertainties at the prevailing operating conditions, propagates them through the full measurement chain, and returns the combined standard uncertainties of the COP, Carnot COP, and Carnot efficiency. Section 5.1 presents and discusses the numerical results across the six operating points. Section 5.2 reports the sensitivity analysis, which isolates the contribution of each input quantity to the total uncertainty. Section 5.3 assesses the results against the reference requirements of DIN EN 14511-3 and derives practical implications for the measurement campaign.

5.1 Performance indicators and combined uncertainties at selected operating points

The measurement uncertainty model developed in Section 4 was evaluated numerically for six representative operating points derived from the simulation study of Höckenkamp et al. [5]. The operating conditions and the resulting performance indicators together with their absolute and relative combined standard uncertainties are summarized in Table 3 and 4.

Table 3. Operating points and combined standard uncertainties of the performance indicators.

No.	$T_{out,S}$ [°C]	$T_{in,S}$ [°C]	$T_{in,Q}$ [°C]	$\dot{m}$ [kg/s]	P_{el} [kW]
1	140	115	80	2.0	45
2	200	175	80	1.7	62
3	200	175	130	6.9	200
4	140	115	130	7.4	95
5	150	125	100	3.6	79
6	180	155	110	4.5	125

Table 4. resulting performance indicators and their relative combined standard uncertainties

No.	COP	$u(COP)$	COP_{Carn}	$u(COP_{Carn})$	η_{Carn}	$u(\eta_{Carn})$
1	4.72	±1.56 %	6.89	±0.096 %	0.67	±1.56 %
2	3.04	±1.49 %	3.94	±0.059 %	0.77	±1.50 %
3	3.82	±1.18 %	6.76	±0.133 %	0.57	±1.18 %
4	8.28	±1.30 %	41.32	±0.772 %	0.20	±1.31 %
5	4.87	±1.36 %	8.46	±0.110 %	0.58	±1.36 %
6	3.92	±1.14 %	6.47	±0.099 %	0.61	±1.14 %

The combined standard uncertainties of the COP range from ±1.14 % to ±1.56 % across the six operating points. The lowest uncertainty occurs at operating point 6, where the mass flow rates and the compressor power approach the respective design points of the instrumentation most closely. The highest uncertainty is observed at operating point 1, which combines a low sink-side temperature difference which increases the relative impact of the PT100 minimum error and with a low compressor power, placing the current transformers further from their optimal load fraction.

The combined uncertainties of the Carnot COP are lower than these of the COP, ranging from ±0.059 % to ±0.772 %. This difference reflects the limited number of input quantities entering Eq. (4) and the high accuracy

of the PT100 sensors at higher temperature differences between sink outlet and source inlet. The exceptional case is operating point 4, where the temperature lift between source inlet (130 °C) and sink outlet (140 °C) is only 10 K. The resulting Carnot COP of 41.32 is thermodynamically plausible but carries a notably elevated relative uncertainty of ±0.772 % since the sensitivity coefficients of Eqs. (20) and (21) scale with the inverse square of the temperature lift.
The combined uncertainties of Carnot efficiency closely mirror those of the COP in all operating points, which is expected from Eq. (7). $u(COP)$ is larger than $u(COP_{Carnot})$, so the Carnot efficiency uncertainty is dominated by the COP contribution.
Compared with published data from analogous systems, the uncertainties obtained here are notably low. Di Wu et al. [12] report operating-point-dependent relative COP uncertainties of ±3.9 % to ±4.7 % for an HTHP of comparable architecture like a water-refrigerant system with a screw compressor and liquid injection. In this scenario their uncertainty is nearly three times the values determined for the SteamScrew test rig. The difference is attributable to the larger individual sensor uncertainties used in that study. Mendes et al. [13] demonstrate that COP uncertainties in the range of ±1.6 % are achievable with high-accuracy instrumentation for a different heat pump type (R-410A, rotary compressor), which is consistent with the upper end of the range found in the present study. The results thus confirm that the instrumentation of the SteamScrew test rig is well-suited to the intended measurement task.

5.2 Sensitivity analysis

A local sensitivity analysis was conducted to quantify the relative influence of each input quantity on the combined uncertainty of the three performance indicators. Starting from the conditions of operating point 6 as the reference, each input parameter was varied individually over a range of ±50 % of its reference value while all other inputs were held constant. For temperature inputs, the variation range was restricted to maintain physically feasible operating conditions within the design envelope of the test rig. The uncertainty of the specific heat capacity varied directly from 0 % to 1 % rather than through an underlying sensor quantity, consistent with its treatment as a literature-based fixed uncertainty.
Sensitivity of $u(COP)$. The mass flow rate has very little influence on $u(COP)$ across the entire variation range. A ±50 % change in mass flow rate shifts $u(COP)$ by less than 0.001 percentage points. This result reflects the exceptionally low uncertainty of the calibrated CMDs in their normal operating range and confirms that the Coriolis meters are not a limiting factor for COP accuracy. The electrical power has a moderate and monotonically decreasing influence. As the compressor power increases from 62.5 kW to 187.5 kW, $u(COP)$ falls from ±1.44 % to ±1.11 %, consistent with the improving accuracy of the current transformers at higher load fractions as shown in Figure 1. The CMD signal conditioning card introduces a non-linear response. The uncertainty of $u(COP)$ is minimised near 25 °C cabinet temperature which is the card calibration point of the card and increases on both sides, reaching ±1.27 % at 60 °C. This case is possible but should not occur during testing.

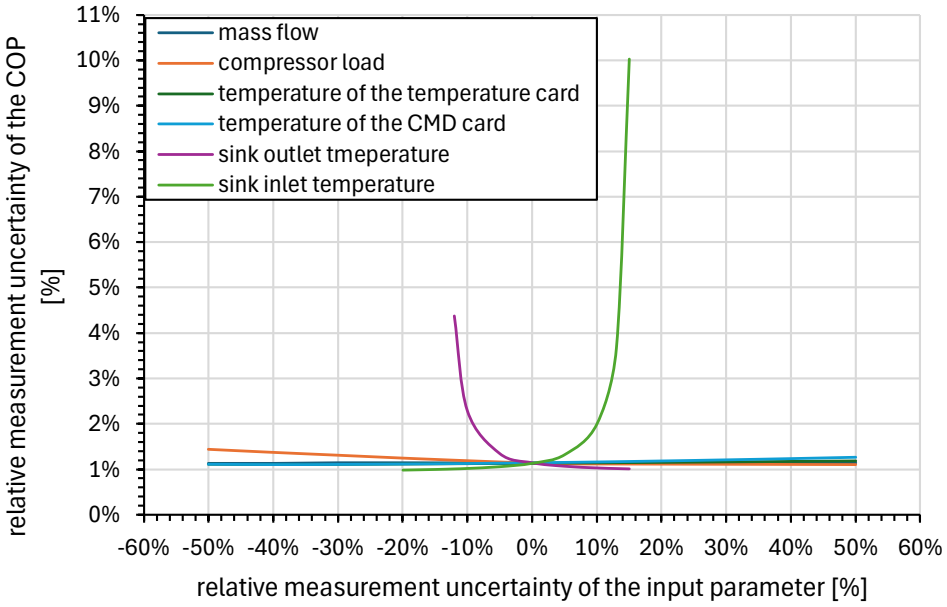

Figure 1. Changes in the total measurement uncertainty of the COP resulting from changes in the input variables

The dominant sensitivity drivers are the sink-side temperatures as shown in figure 1. An increase of the sink inlet temperature by 15 % (from 155 °C to 178.25 °C), which reduces the temperature difference between inlet and outlet to 2.75 K, drives $u(COP)$ to ±10.0 %. Conversely, a decrease in the sink outlet temperature by 15 % raises $u(COP)$ to ±4.4 %. In both cases the sharp rise is caused by the PT100 minimum error of ±0.1 K becoming a large fraction of the small temperature difference, which appears in the numerator of the COP sensitivity coefficients Eqs. (17) and (18). This effect is an important practical constraint on measurement accuracy for the COP determination of any calorimetric heat pump test.

Sensitivity of $u(COP_{Carnot})$. The Carnot COP uncertainty is sensitive only to the two temperature inputs. Minimizing the difference between the two temperatures raises the uncertainty from ±0.1 % in the starting point up to ±0.76 % when the temperature-difference becomes only 15 K as can be seen at the source inlet temperature in Figure 2. The temperature measurement card contributes a comparatively small and approximately linear response over the range considered.

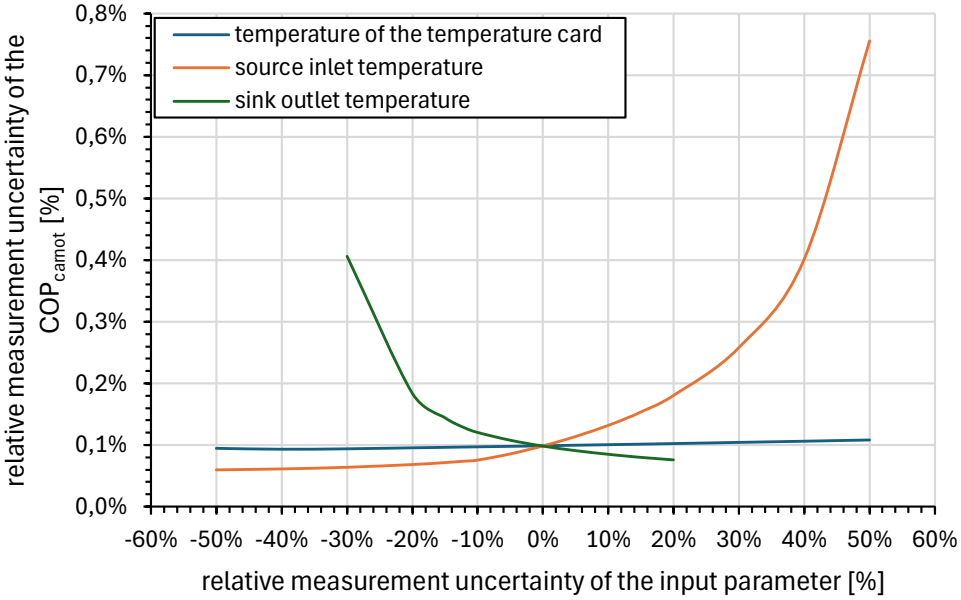

Figure 2. Changes in the total measurement uncertainty of the Carnot COP resulting from changes in the input variables

Sensitivity of $u(\eta_{Carnot})$. The sensitivity structure of the Carnot efficiency mirrors that of COP for all shared input quantities, since $u(COP)$ dominates Eq. (7). The source inlet temperature introduces an additional, slowly rising contribution via $u(COP_{Carnot})$. $u(COP_{Carnot})$ increases from ±1.14 % to ±1.37 % as the source temperature increases from 110 °C to 165 °C. The behavior at small temperature differences is identical to that observed for $u(COP)$, with $u(\eta_{Carnot})$ reaching ±10.0 % when the sink inlet and outlet temperatures converge to within 2.75 K.

5.3 Compliance with measurement standards and practical implications

Although no dedicated measurement standard exists for high-temperature industrial heat pumps, the requirements specified in DIN EN 14511-3 [14] for electrically driven heat pumps intended for space heating provide a relevant reference frame. That standard prescribes maximum allowable measurement uncertainties of ±0.15 K for temperatures, ±1 % for mass flow rates, and ±1 % for electrical power.

Under the boundary conditions of the present analysis, all three requirements are met within the normal operating range of the SteamScrew test rig. The PT100 Class AA sensors satisfy the temperature requirement at all sink-side operating points within the calibrated temperature range. The Coriolis meters satisfy the mass flow requirement at all flow fractions above 20 % of the rated maximum, which encompasses the entire expected operating envelope. The electrical power requirement is satisfied when the compressor operates above approximately 50 % of maximum load. At lower loads, the current transformer uncertainty rises to the margin of compliance, underscoring the importance of selecting transformers rated closer to the actual motor current.

The results also reveal an optimization potential in the signal conditioning hardware. The CMD measurement cards, calibrated at 25 °C, introduce uncertainties of ±0.445 % at the expected cabinet temperature of 40°C. Re-calibrating the cards at 40 °C would eliminate this temperature offset and reduce the combined mass flow uncertainty. Similarly, the installed air conditioning units can reduce temperature deviations from the ideal

conditions. The same argument applies to the temperature measurement cards, though their contribution is proportionally smaller.

6. Conclusion and recommendations

This study presented a systematic measurement uncertainty analysis for the operating-point-dependent performance indicators of the SteamScrew high-temperature heat pump test rig, which uses water as the natural refrigerant and a twin-screw compressor with liquid injection. Analytical uncertainty functions were derived for the COP, the Carnot COP, and the Carnot efficiency by applying Gaussian error propagation to the full measurement chain. The model was evaluated numerically for six representative operating points and complemented by a local sensitivity analysis.

Combined uncertainties are low compared to literature. The combined standard uncertainty of the COP ranges from ±1.14 % to ±1.56 % across the operating points investigated, which is approximately three times lower than the ±3.9 % to ±4.7 % reported by Di Wu et al. [12] for a comparable water-refrigerant screw compressor system. The difference is attributable to the more accurate instrumentation deployed at the SteamScrew test rig, in particular the calibrated Coriolis meters and Class AA PT100 sensors. The values obtained are consistent with the lower bound of ±1.6 % demonstrated by Mendes et al. [13] for a precisely instrumented conventional heat pump. The Carnot COP uncertainty is smaller than the COP uncertainty, ranging from ±0.059% to ±0.772 %, owing to the limited number of input quantities and the high accuracy of the temperature sensors at moderate temperature lifts.

Temperature measurement at small temperature differences is the dominant uncertainty driver. The sensitivity analysis identifies the sink-side temperature difference between condenser inlet and outlet as the critical variable controlling COP accuracy. When this difference falls, the PT100 minimum error of ±0.1 K becomes the dominant uncertainty. This effect is inherent to calorimetric heat output determination and cannot be mitigated by improving any other element of the measurement chain.

Optimization potential in the electrical power measurement chain. The installed AcuCT-S220-1200:5 current transformers have a rated primary current of 1200 A, which exceeds the maximum motor current of the SteamScrew compressor of 409 A. This results in a load fraction of 34 % at full compressor load, a range in which the relative transformer uncertainty is higher than at rated conditions. As the test rig was designed prior to the final determination of the compressor operating range, this constellation represents a natural starting point for future instrumentation refinement. Replacing the current transformers with units of a lower rated primary current would reduce the transformer uncertainty at the design operating point and is identified as a straightforward optimization measure for subsequent measurement campaigns.

Signal conditioning cards calibrated at 25 °C introduce uncertainty at operating temperatures. The temperature and CMD measurement cards are factory-calibrated at a reference temperature of 25 °C, whereas the expected cabinet temperature during operation is 40–60 °C. The resulting temperature offset drives the card uncertainty to ±0.0635 % (temperature card) and ±0.445 % (CMD card) at 40 °C, compared to the minimum values at 25 °C. Re-calibrating the cards at their actual operating temperature would reduce these contributions similarly, also the climate control in the cabinets can help reduce measurement uncertainty.

Sensors operating close to their design points yield the lowest uncertainties. Operating points 3 and 6, in which the mass flow rates, temperatures, and compressor power simultaneously approach the respective design points of the installed instrumentation, produce the lowest COP uncertainties in the study (±1.18 % and ±1.14 %, respectively). This finding underlines the importance of matching sensor specifications to the anticipated operating range during the instrument selection phase of a new test rig.

Auxiliary consumers and electromagnetic compatibility are identified as limitations. The electrical power balance in this study is restricted to the compressor motor. Although the combined power of auxiliary consumers like circulation pumps, actuators, and instrumentation is small relative to the motor power. Their omission introduces a systematic overestimation of the COP that should be addressed in future measurement campaigns. Similarly, the influence of electromagnetic compatibility could not be quantified in the present work because the final cable routing was not yet defined at the time of the study. Both aspects can be pursued to enhance the precision of the experimental data.

Outlook. The uncertainty model developed here will be directly applied to process the experimental data acquired during commissioning and initial operation of the SteamScrew test rig. The results will enable a statistically rigorous comparison of the measured performance with simulation predictions and with published data from comparable systems. In parallel, the sensitivity analysis provides a prioritized list of hardware improvements like transformer replacement and auxiliary power metering that can be implemented iteratively as the test program progresses. Furthermore, the analytical framework is sufficiently general to be adapted to other calorimetric heat pump test rigs.

Acknowledgments

This work was carried out within the joint research project SteamScrew, which is funded by the German Federal Ministry for Economic Affairs and Climate Action (Bundesministerium für Wirtschaft und Klimaschutz, BMWK) under grant number 03EN4048A with a total funding volume of 2.6 million euros. The project runs from January 2023 to June 2026.

The authors gratefully acknowledge the contributions of the project partners: the Department of Fluid Technology (Fachgebiet Fluidtechnik) at TU Dortmund University, which is responsible for the simulation and experimental validation of the compressor, and Aerzener Maschinenfabrik GmbH, which developed and constructed the twin-screw compressor. The integration and operation of the heat pump test rig at laboratory scale is conducted at the Fraunhofer Research Institution for Energy Infrastructures and Geotechnologies IEG in Bochum.

References

[1] Naegler T, Simon S, Klein M, Gils HC. Potenziale für erneuerbare Energien in der industriellen Wärmeerzeugung; 2012. Available from: URL: https://core.ac.uk/download/pdf/77229329.pdf.

[2] Arpagaus C. Hochtemperatur Wärmepumpen: Literaturstudie zum Stand der Technik, der Forschung, des Anwendungspotenzials und der Kältemittel 2020.

[3] Lerch R. Elektrische Messtechnik: Analoge, digitale und computergestützte Verfahren. Berlin, Heidelberg: Springer 2016.

[4] Fraunhofer IEG. Entwicklung einer Hochtemperatur-Wärmepumpe mit Wasserdampf-Schraubenverdichter zur Wärme- und Prozessdampfbereitstellung »SteamScrew«; 2025 [cited 2025 December 1] Available from: URL: https://www.ieg.fraunhofer.de/de/projekte/SteamScrew.html.

[5] Höckenkamp S, Grieb M, Utri M, Brümmer A. Performance Analysis of a Water-Injected Twin-Screw Compressor in a High-Temperature R718 Heat Pump. IOP Conf. Ser.: Mater. Sci. Eng. 2024; 1322(1): 12018 [https://doi.org/10.1088/1757-899X/1322/1/012018]

[6] Zok AP. Thermodynamische Simulation eines Hochtemperatur-Wärmepumpenkreislaufs mit Wasser als Kältemittel in Modelica. MasterarbeitRuhruniversität Bochum 2024 May 10.

[7] Dohmann J. Thermodynamik der Kälteanlagen und Wärmepumpen. Berlin, Heidelberg: Springer Berlin Heidelberg 2016.

[8] Bell IH, Wronski J, Quoilin S, Lemort V. Pure and Pseudo-pure Fluid Thermophysical Property Evaluation and the Open-Source Thermophysical Property Library CoolProp. Industrial & Engineering Chemistry Research 2014; 53(6): 2498–508 [https://doi.org/10.1021/ie4033999]

[9] Eder W, Moser F, Kögl B. Die Wärmepumpe in der Verfahrenstechnik. Springer-Verlag 1979.

[10] Deutsches Institut für Normung (DIN). Industrielle Platin-Widerstandsthermometer und Platin-Temperatursensoren: Deutsche Fassung EN_IEC_60751:2022. Berlin: DIN Media GmbH; 2023 2023-06.

[11] Deutsches Institut für Normung (DIN). Messwandler - Teil 2: Zusätzliche Anforderungen für Stromwandler (IEC 61869-2:2012): Deutsche Fassung EN 61869-2:2012, Berichtigung zu DIN EN 61869-2 (VDE 0414-9-2):2013-07. DIN Media GmbH; 2014 2014-06.

[12] Di Wu, Jiang J, Hu B, Wang RZ. Experimental investigation on the performance of a very high temperature heat pump with water refrigerant. Energy 2020; (190) [https://doi.org/10.1016/j.energy.2019.116427]

[13] Mendes N, Moura LM, Reichenbach Pizzatto L. Measurement Uncertainties Calculation in the cooling Capacity Determination of split air Conditioners by the air-enthalpy Methology. In: Measurement Uncertainties Calculation in the cooling Capacity Determination of split air Conditioners by the air-enthalpy Methology; 2017. ABCM.

[14] Deutsches Institut für Normung (DIN). Luftkonditionierer, Flüssigkeitskühlsätze und Wärmepumpen für die Raumbeheizung und -kühlung und Prozesskühler mit elektrisch angetriebenen Verdichtern - Teil 3: Prüfverfahren. DIN Media GmbH; 2023 2023-12.